# The quench action approach for integrable models: A Monte Carlo implementation

**Authors**

**Abstract.**
fdasfa

## 1. Introduction

We show that it is possible to numerically simulate the Quench Action approach combining Monte Carlo methods and Bethe ansatz techniques.
We focus on the situation in which the pre-quench initial state is the Neel state or the Majumdar-Ghosh state.
We investigate the importance of the zero-momentum strings in the Quench Action.
Without zero-momentum strings the overlap saturation rules are not valid, i.e., in finite size systems the vast majority of the eigenstates contain zero momentum strings.
The details on the eigenstates counting depend on the pre-quench initial state.
However, we show that one can restrict to the set of non-zero momentum strings. The fact that one neglects zero-momentum strings gives rise only to scaling corrections.
We also investigate the validity of the Bethe-Takahashi approximation for the calculation of the overlap.
In the thermodynamic limit it is natural to assume that the steady-state expectation values are obtained using the so-called diagonal ensemble, which is defined as

$$\langle \mathcal{O} \rangle = \sum_{\alpha} |\langle \Psi_0 | \alpha \rangle|^2 \langle \alpha | \mathcal{O} | \alpha \rangle. \tag{1}$$

It is useful to rewrite (1) as

$$\langle \mathcal{O} \rangle = \sum_{\alpha} \rho^{DE}(\alpha) \langle \alpha | \mathcal{O} | \alpha \rangle, \quad \text{with} \quad \rho^{DE}(\alpha) = \exp(-2\Re \mathcal{E}(\alpha)). \tag{2}$$

Here $\rho^{DE}(\alpha)$ is a diagonal ensemble density matrix, and $\mathcal{E}(\alpha) \equiv -\log\langle \alpha | \Psi_0 \rangle$, with $\Re$ denoting the real part.

## 2. Bethe ansatz solution of the Heisenberg ($XXX$) spin chain

Here we review some Bethe ansatz results for the spin-$\frac{1}{2}$ Heisenberg ($XXX$) chain. Specifically, in section 2.1 we introduce the model. Its eigenstates (Bethe states) and the Bethe equations are discussed in section 2.2. Section 2.3 focuses on the string hypothesis and the so-called Bethe-Gaudin-Takahashi (BGT) equations. The form of the BGT equations in the thermodynamic limit is discussed in section 2.4. Finally, in section 2.5 we provide some exact formulas for the local conserved charges of the model.

### *2.1. The spin-$\frac{1}{2}$ Heisenberg chain*

The spin-$\frac{1}{2}$ isotropic Heisenberg chain ($XXX$ chain) with $L$ sites is defined by the Hamiltonian

$$\mathcal{H} \equiv J \sum_{i=1}^{L} \left[ \frac{1}{2}(S_i^+ S_{i+1}^- + S_i^- S_{i+1}^+) + S_i^z S_{i+1}^z - \frac{1}{4} \right], \tag{3}$$

where $S_i^{\pm} \equiv (\sigma_i^x \pm i\sigma_i^y)/2$ are spin operators acting on the site $i$, $S_i^z \equiv \sigma_i^z/2$, and $\sigma_i^{x,y,z}$ the Pauli matrices. We fix $J = 1$ and use periodic boundary conditions, identifying sites

$L+1$ and 1. The total magnetization $S^z_T \equiv \sum_i S^z_i = L/2 - M$, with $M$ number of down spins (particles), commutes with (3), and it is here used to label its eigenstates.

### *2.2. Bethe equations and wavefunctions*

In the Bethe ansatz framework [19, 20] the generic eigenstate of (3) (Bethe state) in the sector with $M$ particles can be written as

$$|\Psi_M\rangle = \sum_{1\leq x_1<x_2<\ldots<x_M\leq L} A_M(x_1, x_2, \ldots, x_M)|x_1, x_2, \ldots, x_M\rangle, \tag{4}$$

where the sum is over the positions $\{x_i\}_{i=1}^M$ of the particles, and $A_M(x_1, x_2, \ldots, x_M)$ is the eigenstate amplitude corresponding to the particles being at positions $x_1, x_2, \ldots, x_M$. Here $A_M(x_1, x_2, \ldots, x_M)$ is given as

$$A_M(x_1, x_2, \ldots, x_M) \equiv \sum_{\sigma\in S_M} \exp\Big[i\sum_{j=1}^M k_{\sigma_j}x_j + i\sum_{i<j}\theta_{\sigma_i,\sigma_j}\Big], \tag{5}$$

where the outermost summation is over the permutations $S_M$ of the so-called quasi-momenta $\{k_\alpha\}_{\alpha=1}^M$. The two-particle scattering phases $\theta_{\alpha,\beta}$ are defined as

$$\theta_{\alpha,\beta} \equiv \frac{1}{2i}\log\Big[-\frac{e^{ik_\alpha+ik_\beta} - 2e^{ik_\alpha} + 1}{e^{ik_\alpha+ik_\beta} - 2e^{ik_\beta} + 1}\Big]. \tag{6}$$

The eigenenergy associated to the eigenstate (4) is

$$E = \sum_{\alpha=1}^M(\cos(k_\alpha) - 1). \tag{7}$$

The quasi-momenta $k_\alpha$ are obtained by solving the so-called Bethe equations [19]

$$e^{ik_\alpha L} = \prod_{\beta\neq\alpha}^M\Big[-\frac{1 - 2e^{ik_\alpha} - e^{ik_\alpha+ik_\beta}}{1 - 2e^{ik_\beta} - e^{ik_\alpha+ik_\beta}}\Big]. \tag{8}$$

It is useful to introduce the rapidities $\{\lambda_\alpha\}_{\alpha=1}^M$ as

$$k_\alpha = \pi - 2\arctan(\lambda_\alpha) \mod 2\pi. \tag{9}$$

Taking the logarithm on both sides in (8), and using (9), one obtains the Bethe equations in logarithmic form as

$$\arctan(\lambda_\alpha) = \frac{\pi}{L}J_\alpha + \frac{1}{L}\sum_{\beta\neq\alpha}\arctan\Big(\frac{\lambda_\alpha - \lambda_\beta}{2}\Big), \tag{10}$$

where $-L/2 < J_\alpha \leq L/2$ are the so-called Bethe quantum numbers. The $J_\alpha$ are half-integers and integers for $L - M$ even and odd, respectively.

Finally, one should remark that $M$-particle eigenstates corresponding to *finite* rapidities are eigenstates with maximum allowed magnetization (highest-weight eigenstates) $S^z_T = L/2 - M = S_T$, with $S_T$ the total spin. Due to the $SU(2)$ invariance of (3), all the states in the same $S_T$ multiplet and different $-S_T \leq S^z_T \leq S_T$ are eigenstates of the $XXX$ chain with the same energy eigenvalue. These eigenstates (descendants) are

obtained by multiple applications of the total-spin lowering operator $S_T^- \equiv \sum_i S_i^-$ on the highest-weight eigenstates. In the Bethe ansatz framework the rapidities of a generic $M$-particle descendant eigenstate with $S_T^T = L/2 - M'$, with $M' < M$, are obtained by supplementing the $M$ rapidities of the highest-weight state with $M' - M$ infinite rapidities. We anticipate that descendant eigenstates have non-zero overlap with the zero-momentum Néel state (cf. section 3).

### *2.3. String hypothesis & the Bethe-Gaudin-Takahashi (BGT) equations*

In the thermodynamic limit $L \to \infty$ the solutions of the Bethe equations (8) form particular "string" patterns in the complex plane, (string hypothesis) [19, 20]. Specifically, the rapidities forming a "string" of length $1 \leq n \leq M$ (that we defined here as $n$-string) can be parametrized as

$$\lambda_{n;\gamma}^j = \lambda_{n;\gamma} - i(n-1-2j) + i\delta_{n;\gamma}^j, \qquad j = 0, 1, \ldots, n-1, \tag{11}$$

with $\lambda_{n;\gamma}$ being the real part of the string (string center), $\gamma$ labelling strings with different centers, and $j$ labelling the different components of the string. In Eq. (11) $\delta_{n;\gamma}^j$ are the string deviations, which typically, i.e., for most of the chain eigenstates, vanish exponentially with $L$ in the thermodynamic limit. Note that real rapidities correspond to strings of unit length (1-strings), i.e., $n = 1$ in Eq. (11).

The string centers $\lambda_{n;\gamma}$ are obtained by solving the so-called Bethe-Gaudin-Takahashi equations

$$2L\theta_n(\lambda_{n;\gamma}) = 2\pi I_{n;\gamma} + \sum_{(m,\beta)\neq(n,\gamma)} \Theta_{m,n}(\lambda_{n;\gamma} - \lambda_{m;\beta}). \tag{12}$$

The generalized scattering phases $\Theta_{m,n}$ read

$$\Theta_{m,n}(x) \equiv \begin{cases} \theta_{|n-m|}(x) + \sum_{r=1}^{(n+m-|n-m|-1)/2} 2\theta_{|n-m|+2r}(x) + \theta_{n+m}(x) & \text{if} \quad n \neq m \\ \sum_{r=1}^{n-1} 2\theta_{2r}(x) + \theta_{2n}(x) & \text{if} \quad n = m \end{cases}$$

with $\theta_\alpha(x) \equiv 2\arctan(x/\alpha)$. Here $I_{n;\gamma}$ are the Bethe-Takahashi quantum numbers associated with $\lambda_{n;\gamma}$. The solutions of (12), and the Bethe states thereof, are naturally classified according to their "string content" $\mathcal{S} \equiv \{s_n\}_{n=1}^M$, with $s_n$ the number of $n$-strings. Clearly, the constraint $\sum_{n=1}^M n s_n = M$ has to be satisfied. It can be shown that the BGT quantum numbers $I_{n;\gamma}$ associated with the $n$-strings are integers and half-integers for $L - s_n$ odd and even, respectively. An upper bound for the BGT quantum numbers can be derived as [20]

$$|I_{n;\gamma}| \leq I_n^{(MAX)} \equiv \frac{1}{2}(L - 1 - \sum_{m=1}^M t_{m,n} s_m), \tag{13}$$

where $t_{m,n} \equiv 2\min(n,m) - \delta_{m,n}$. Using the string hypothesis Bethe states energy eigenvalue (7) becomes

$$E = -\sum_{n,\gamma} \frac{2n}{\lambda_{n;\gamma}^2 + n^2}. \tag{14}$$

### *2.4. Thermodynamic limit*

In the thermodynamic limit $L \to \infty$ at fixed finite particle density $M/L$ the solutions of the BGT equations (12) become dense. One then defines the BGT root distributions for the $n$-strings as $\boldsymbol{\rho} \equiv \{\rho_n(\lambda)\}_{n=1}^{\infty}$, with $\rho_n(\lambda) \equiv \lim_{L\to\infty}[\lambda_{n;\gamma+1} - \lambda_{n;\gamma}]^{-1}$. Thus the BGT equations (12) become an infinite set of coupled non-linear integral equations for the $\rho_n(\lambda)$ as

$$a_n(\lambda) = \rho_n(\lambda) + \rho_n^h(\lambda) + \sum_m (T_{n,m} * \rho_m)(\lambda), \tag{15}$$

where $\rho_n^h$ are the hole-distributions, and the functions $a_n(\lambda)$ are defined as

$$a_n(x) \equiv \frac{1}{\pi}\frac{n}{x^2+n^2}. \tag{16}$$

In (15) $T_{n,m} * \rho_m$ denotes the convolution

$$(T_{n,m} * \rho_m)(\lambda) \equiv \int_{-\infty}^{+\infty} T_{n,m}(\lambda - \lambda')\rho_m(\lambda'), \tag{17}$$

with the matrix $T_{n,m}(x) \equiv \Theta'(x)$ being dfined as

$$T_{m,n}(x) \equiv \begin{cases} a_{|n-m|}(x) + \sum_{r=1}^{(n+m-|n-m|-1)/2} 2a_{|n-m|+2r}(x) + a_{n+m}(x) & \text{if} \quad n \neq m \\ \sum_{r=1}^{n-1} 2a_{2r}(x) + a_{2n}(x) & \text{if} \quad n = m \end{cases}$$

For a generic smooth enough observable $\mathcal{O}$ in the thermodynamic limtit its expectation value is expected to become a functional of the root densities $\boldsymbol{\rho}$ as $\langle\boldsymbol{\rho}|\mathcal{O}|\boldsymbol{\rho}\rangle$.
Moreover, for all the local observables considered in this work the contribution of the different type of strings factorize and one can write

$$\langle\boldsymbol{\rho}|\mathcal{O}|\boldsymbol{\rho}\rangle = \sum_{n=1}^{\infty}\int_{-\infty}^{+\infty} d\lambda \rho_n(\lambda)\mathcal{O}_n(\lambda), \tag{18}$$

with $\mathcal{O}_n(\lambda)$ the ... .

### *2.5. The conserved charges*

The $XXX$ chain exhibits an extensive number of mutually commuting local conserved charges $Q_n$, with $n \in \mathbb{N}$, i.e.,

$$[Q_n, \mathcal{H}] = 0 \quad \forall n \quad \text{and} \quad [Q_n, Q_m] = 0 \quad \forall n, m. \tag{19}$$

The eigenvalues $q_n$ of the conserved charges over the Bethe eigenstates (cf. (4)) are given as

$$q_{n+1} \equiv \frac{i}{(n-1)!}\frac{d^n}{dy^n}\log\tau(y)\Big|_{y=i}, \tag{20}$$

where $y$ is a spectral parameter and $\tau(y)$ is the Bethe state eigenvalue of the so-called transfer matrix in the Algebraic Bethe Ansatz framework [21]. The analytic expression for $\tau(y)$ in terms of the solutions $\{\lambda_\alpha\}_{\alpha=1}^{M}$ of the Bethe equations (8) is given as

$$\tau(y) \equiv \Big(\frac{y+i}{2}\Big)^L \prod_\alpha \frac{y-\lambda_\alpha-2i}{y-\lambda_\alpha} + \Big(\frac{y-i}{2}\Big)^L \prod_\alpha \frac{y-\lambda_\alpha+2i}{y-\lambda_\alpha}. \tag{21}$$

Interestingly, from (20) one has that the second term in (21) does not contribute to $q_n$, at least for $n \leq L-2$. For a generic Bethe state $q_n$ is obtained by summing independently the contributions of the BGT roots as

$$q_n = \sum_{k,\gamma} g_{n,k}(\lambda_{k;\gamma}). \tag{22}$$

Using the string hypothesis (11), and (20), (21), one obtains the the first few functions $g_{n,k}$ in terms of the solutions of the BGT equations as

$$\begin{aligned} g_{3,k} &= -\frac{4k\lambda_{k;\gamma}}{(\lambda_{k;\gamma}^2+k^2)^2}, \qquad g_{4,k} = \frac{2k(k^2-3\lambda_{k;\gamma}^2)}{(k^2+\lambda_{k;\gamma}^2)^3} \\ g_{5,k} &= \frac{8k\lambda_{k;\gamma}(k^2-\lambda_{k;\gamma}^2)}{(k^2+\lambda_{k;\gamma}^2)^4}, \quad g_{6,k} = -\frac{2k(5\lambda_{k;\gamma}^4-10k^2\lambda_{k;\gamma}^2+k^4)}{(k^2+\lambda_{k;\gamma}^2)^5}. \end{aligned} \tag{23}$$

Note that $q_2$ is the Bethe state energy eigenvalue and is given in (14). It is also interesting to observe that $g_{n,k}$ (cf. (23)) is vanishing for infinite BGT roots. This is expected to hold for the generic $g_{n,k}$, i.e., for any $n$, and it is a consequence of the $SU(2)$ invariance of the conserved charges. Finally, in the thermodynamic limit $L \to \infty$ from (22) one has

$$q_n \to \sum_{k=1}^{\infty} \int_{-\infty}^{+\infty} d\lambda \rho_k(\lambda) g_{n,k}(\lambda), \tag{24}$$

where the BGT root distributions $\rho_k(\lambda)$ are solutions of (15).

## 3. Overlap between the Bethe states and some initial states

### *3.1. Néel state overlap*

Here we detail the Bethe ansatz results for the overlap of the Bethe states (cf. (4)) with the zero-momentum (one-site shift invariant) Néel state $|N\rangle$ and the Majumdar-Ghosh (MG) $|MG\rangle$ state. We stard discussing the Néel state. This is defined as

$$|N\rangle \equiv \frac{1}{\sqrt{2}}(|N_1\rangle + |N_2\rangle), \tag{25}$$

with $|N_1\rangle \equiv |\uparrow\downarrow\rangle^{\otimes L/2}$, and $|N_2\rangle \equiv |\downarrow\uparrow\rangle^{\otimes L/2}$. Note that $|N_1\rangle = \hat{T}|N_2\rangle$, with $\hat{T}$ the one-site shift operator.

Due to the zero-momentum constraint, only parity-invariant Bethe states can have non-zero Néel overlap [22]. Parity-invariant Bethe states contain only pairs of solutions of the Bethe equations (8) with opposite sign. Here we denote the generic parity-invariant rapidity configuration as $|\{\pm\tilde{\lambda}_\alpha\}_{\alpha=1}^m, n_\infty\rangle$, i.e., considering only positive rapidities. Here $m$ is the number of rapidity pairs. Since the Néel state is not invariant under $SU(2)$ rotations, eigenstates with infinite rapidities can have non-zero Néel overlaps. Here the number of infinite rapidities is denoted as $N_\infty$. Note that one has $M = L/2 = N_\infty + 2m$.

We denote as $n_\infty \equiv N_\infty/L$ the density of infinite rapidities. Finally, the overlap between the Bethe states and the Neel state $|N\rangle$ reads [22, 29]

$$\frac{\langle N|\{\pm\tilde{\lambda}_j\}_{j=1}^m, n_\infty\rangle}{|||\{\tilde{\lambda}_j\}_{j=1}^m, n_\infty\rangle||} = \frac{\sqrt{2}N_\infty!}{\sqrt{(2N_\infty)!}}\left[\prod_{j=1}^m \frac{\sqrt{\tilde{\lambda}_j^2+1}}{4\tilde{\lambda}_j}\right]\sqrt{\frac{\det_m(G^+)}{\det_m(G^-)}}. \tag{26}$$

The matrix $G^\pm$ is defined as

$$G^\pm_{jk} = \delta_{jk}\Big(LK_{1/2}(\tilde{\lambda}_j) - \sum_{l=1}^m K_1^+(\tilde{\lambda}_j,\tilde{\lambda}_l)\Big) + K_1^\pm(\tilde{\lambda}_j,\tilde{\lambda}_k), \quad j,k=1,\dots,m, \tag{27}$$

where

$$K_1^\pm(\lambda,\mu) = K_1(\lambda-\mu) \pm K_1(\lambda+\mu) \quad \text{with} \quad K_\alpha(\lambda) \equiv \frac{8\alpha}{\lambda^2+4\alpha^2}. \tag{28}$$

Note that our definitions of $K_\alpha(\lambda)$ differs from the one in Ref. [22], due to a factor 2 in the definition of the rapidities (see also (11)).

### *3.2. The string hypothesis: Reduced Néel overlap formulas*

Here we consider the overlap formula for the Neel state (26) in the limit $L\to\infty$, assuming that the rapidities form perfect strings, i.e., $\delta^j_{n;\gamma}=0$ in (11). Then it is possible to rewrite (26) in terms of the string centers $\tilde{\lambda}_{n;\alpha}$ only. Here we restrict ourselves to rapidity configurations with no zero-momentum strings, i.e., with finite string centers. Our results are not valid for zero-momentum strings.

First, we restrict ourselves to parity-invariant string configurations, i.e., considering only strings having positve string centers. We denote the generic parity-invariant string configuration as $\{\tilde{\lambda}_{n;\gamma}\}$, where $\gamma$ labels the different non-zero string centers, and $n$ is the string length.

It is convenient to first split the indices $i,j$ of $G^\pm_{ij}$ as $i=(n,\gamma,i)$ and $j=(m,\gamma',j)$, with $n,m$ being the length of the strings, $\gamma,\gamma'$ labelling the corresponding string centers, and $i,j$ the components of the two strings.

Using (27) and (28), one has that for two consecutive rapidities in the same string, i.e., for $m=n,\gamma=\gamma',|i-j|=2$, the matrices $G^\pm_{jk}$ become ill-defined in the thermodynamic limit. Precisely, since $K_1(\tilde{\lambda}^i_{n;\gamma}-\tilde{\lambda}^{i+1}_{n;\gamma})\sim 1/(\delta^i_{n;\gamma}-\delta^{i+1}_{n;\gamma})$, $G^\pm_{ij}$ diverges in the thermodynamic limit. Importantly, as the same type of divergence occur in both $G^+$ and $G^-$, their ratio (cf. (26)), and the overlaps, are finite.

The finite part of the overlaps (26) can be calculated using the same strategy as in Ref. [26, 27] (see also Ref. [22]). The resulting matrix $G^+$ depends only on the "string center" indices $(n,\gamma)$ and $(m,\gamma')$ and it is given as

$$\frac{1}{2}G^+_{(n,\gamma)(m,\gamma')} = \begin{cases} L\theta'_n(\tilde{\lambda}_{n;\gamma}) - \sum\limits_{(\ell,\alpha)\neq(n,\gamma)}\Big[\Theta'_{n,\ell}(\tilde{\lambda}_{n;\gamma}-\tilde{\lambda}_{\ell;\alpha}) \\ \qquad +\Theta'_{n,\ell}(\tilde{\lambda}_{n;\gamma}+\tilde{\lambda}_{\ell;\alpha})\Big] & \text{if } (n,\gamma)=(m,\gamma') \\ \Theta'_{n,m}(\tilde{\lambda}_{n;\gamma}-\tilde{\lambda}_{m;\gamma'}) + \Theta'_{n,m}(\tilde{\lambda}_{n;\gamma}+\tilde{\lambda}_{m;\gamma'}) & \text{if } (n,\gamma)\neq(m,\gamma') \end{cases} \tag{29}$$

Here $\theta_n'(x) \equiv d\theta_n(x)/dx = 2n/(n^2+x^2)$ and $\Theta'(x) \equiv d\Theta(x)/dx$, with $\Theta(x)$ as defined in (13). Similarly, for $G^-$ one obtains

$$\frac{1}{2}G^-_{(n,\gamma)(m,\gamma')} = \begin{cases} (L-1)\theta_n'(\tilde{\lambda}_{n;\gamma}) - 2\sum_{k=1}^{n-1}\theta_k'(\tilde{\lambda}_{n;\gamma}) & \text{if } (n,\gamma)=(m,\gamma') \\ -\sum_{(\ell,\alpha)\neq(n,\gamma)}\Big[\Theta'_{n,\ell}(\tilde{\lambda}_{n;\gamma}-\tilde{\lambda}_{\ell;\alpha}) + \Theta'_{n,\ell}(\tilde{\lambda}_{n;\gamma}+\tilde{\lambda}_{\ell;\alpha})\Big] & \\ \quad \Theta'_{n,m}(\tilde{\lambda}_{n;\gamma}-\tilde{\lambda}_{m;\gamma'}) - \Theta'_{n,m}(\tilde{\lambda}_{n;\gamma'}+\tilde{\lambda}_{m;\gamma'})) & \text{if } (n,\gamma)\neq(m,\gamma') \end{cases} \tag{30}$$

Note that in presence of zero-momentum strings, additional divergences as $1/(\delta^i_{n;\gamma}+\delta^{i+1}_{n;\gamma})$ appear due to the term $K_1(\lambda+\mu)$ (cf. (28)). It turns out that the treatment of these diverges is a challenging task because it requires the precise knowledge of the string deviations, meaning their dependence on $L$, for each different type of string. Some results have been provided for small strings in Ref. [17].

Finally, using the string hypothesis and the parity-invariance condition, the multiplicative prefactor in (26) can be simplified. Here we focus on a generic eigenstate of the $XXX$ identified by $m$ pairs of finite rapidities. Note that due to parity invariance and the exclusion of zero-momentum strings, only strings of length up to $m$ are allowed. The "reduced" string content identifying the eigenstate is denoted as $\widetilde{\mathcal{S}} = \{\tilde{s}_1,\dots,\tilde{s}_m\}$, with $\tilde{s}_n$ the number of parity-invariant pairs of $n$-strings. Using the string hypothesis and (26), one can write

$$\prod_{j=1}^{m}\frac{\sqrt{\tilde{\lambda}_j^2+1}}{4\tilde{\lambda}_j} = \frac{1}{4^m}\prod_{j=1}^{m}\prod_{\ell=1}^{\tilde{s}_j}\left[\frac{\sqrt{j^2+\lambda_{j;\ell}^2}}{\lambda_{j;\ell}}\prod_{k=0}^{\lceil j/2\rceil-1}\frac{(2k)^2+\lambda_{j;\ell}^2}{(2k+1)^2+\lambda_{j;\ell}^2}\right]^{(-1)^j}. \tag{31}$$

### *3.3. Overlap with the Majumdar-Ghosh state*

The Majumdar-Ghosh state $|MG\rangle$ is defined as

$$|MG\rangle \equiv \Big(\frac{|\uparrow\downarrow\rangle - |\downarrow\uparrow\rangle}{\sqrt{2}}\Big)^{\otimes L/2}. \tag{32}$$

The overlap between a generic eigenstate of the $XXX$ chain and the Majumdar-Ghosh state can be obtained from the Néel state overlap in Eq. (26) as [29]

$$\langle MG|\{\pm\lambda_j\}_{j=1}^m\rangle = \prod_{j=1}^{m}\frac{1}{2}\Big(1-\frac{\lambda_j-i}{\lambda_j+i}\Big)\Big(1+\frac{\lambda_j+i}{\lambda_j-i}\Big)\langle N|\{\pm\lambda_j\}_{j=1}^m\rangle \tag{33}$$

The mutliplicative factor in (33), using the string hypothesis is rewritten as

$$\prod_{j=1}^{m}\frac{1}{2}\Big(1-\frac{\lambda_j-i}{\lambda_j+i}\Big)\Big(1+\frac{\lambda_j+i}{\lambda_j-i}\Big) = \tag{34}$$

$$2^m\prod_{j=1}^{m}\prod_{\ell=1}^{\tilde{s}_j}\lambda_{j;\ell}^{1+(-1)^j}(\lambda_{j;\ell}^2+j^2)\prod_{k=0}^{\lfloor j/2\rfloor}\Big[\lambda_{j;\ell}^2+\Big(2k+\frac{1-(-1)^j}{2}\Big)^2\Big]^{-2}$$

### *3.4. The Néel overlap in the thermodynamic limit*

In the thermodynamic limit $L \to \infty$ the expression for the extensive part of the overlap (26) can be written as [22]

$$-\lim_{L\to\infty} \log\left[\frac{\langle N|\{\pm\lambda_j\}_{j=1}^m, n_\infty\rangle}{|||\{\lambda_j\}_{j=1}^m, n_\infty\rangle||}\right] = \frac{L}{2}\Big(n_\infty \log 2 + \sum_{n=1}^{\infty}\int_0^\infty d\lambda \rho_n(\lambda)[g_n(\lambda) + 2n\log(4)]\Big), \quad (35)$$

where

$$g_n(\lambda) = \sum_{l=1}^{n-1}\Big[f_{n-1-2l}(\lambda) - f_{n-2l}(\lambda)\Big], \quad \text{with} \quad f_n(\lambda) = \log\left(\lambda^2 + \frac{n^2}{4}\right), \quad (36)$$

and

$$n_\infty = 1 - 2\sum_{m=1}^{\infty} m\int_{-\infty}^{\infty} d\lambda \rho_m(\lambda). \quad (37)$$

Note that (35) is extensive. Specifically, in Eq. (35) subleading (i.e., subextensive) contributions originating from the determinant ratio $\det_m(G^+)/\det_m(G^-)$ are neglected. Moreover, the term in (35) acts as a driving term in the Quech Action formalism (cf. section 4).

## 4. Quench Action treatment of the steady state

In the thermodynamic limit the sum over the model eigenstates in (1) can be recast into a functional integral over the BGT root distributions $\boldsymbol{\rho} \equiv \{\rho_n(\lambda)\}_{n=1}^\infty$ (cf. section 2.4) as

$$\sum_\alpha \to \int \mathcal{D}\boldsymbol{\rho} e^{S_{YY}(\boldsymbol{\rho})}. \quad (38)$$

Here $\mathcal{D}\boldsymbol{\rho} \equiv \prod_{n=1}^\infty \mathcal{D}\rho_n(\lambda)$, $\rho_n(\lambda)$, and $S_{YY}(\boldsymbol{\rho})$ is the Yang-Yang entropy, which counts the number of Bethe states leading to the same $\boldsymbol{\rho}$ in the thermodynamic limit. Using (38), for a generic observable $\mathcal{O}$, its diagonal ensemble expectation value (1) becomes

$$\langle\mathcal{O}\rangle = \int \mathcal{D}\boldsymbol{\rho} \exp\Big[2\Re\log\langle\Psi_0|\boldsymbol{\rho}\rangle + S_{YY}(\boldsymbol{\rho})\Big]\langle\boldsymbol{\rho}|\mathcal{O}|\boldsymbol{\rho}\rangle \quad (39)$$

Here it is assumed that in the thermodynamic limit the eigenstate expectation values $\langle\alpha|\mathcal{O}|\alpha\rangle$ (cf. (1)) and the overlaps $\langle\Psi_0|\boldsymbol{\rho}\rangle$ become smooth functionals of the root distributions $\boldsymbol{\rho}$.

The functional integral in (39) can be evaluated in the limit $L \to \infty$ using the saddle point approximation. One has to minimize the functional $\mathcal{F}(\boldsymbol{\rho})$ defined as

$$L\mathcal{F}(\boldsymbol{\rho}) \equiv 2\Re\log\langle\boldsymbol{\rho}|\Psi_0\rangle + S_{YY}(\boldsymbol{\rho}(\lambda)) \quad (40)$$

with respect to $\boldsymbol{\rho}$, under the constraint that the thermodynamic BGT equations (15) hold. Remarkably, for the quench with initial state the Néel state $|\Psi_0\rangle = |N\rangle$ the

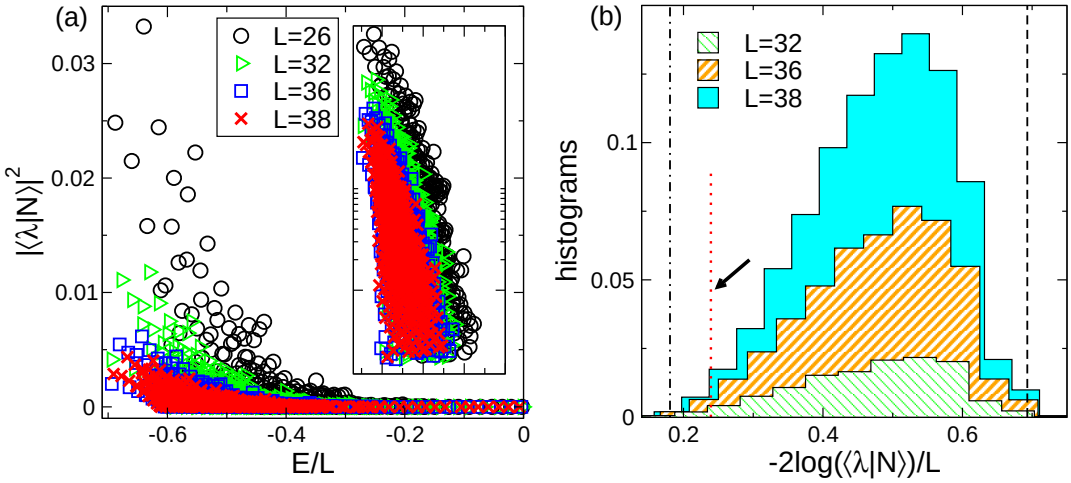


**Figure 1.** Néel state overlaps in the Heisenberg spin chain. (a) The Néel state overlaps with the eigenstates of the Heisenberg spin chain: Squared overlaps $|\langle\lambda|N\rangle|^2$ plotted as a function of the eigenstates energy density $E/L$. Here $|\lambda\rangle$ denotes the generic eigenstate of the Heisenberg spin chain. The data are for chains with length $26 \leq L \leq 38$. The data are obtained from a full scanning of the chains Hilbert space. Eigenstates containing strings with zero-momentum components are escluded. The overlaps decay exponentially with the chain size. (b) Histograms of $-2\log|\langle\lambda|N\rangle|/L$. Different histograms are for different chain sizes. The histogram bin width is $\sim 2/L$. The $y$-axis is rescaled by a factor $10^5$ for convenience. Note the peaking of the histograms around $-2\log|\langle\lambda|N\rangle| \sim 0.5$ in the thermodynamic limit **really??**. The dotted vertical line is the expected Quench-Action result in the thermodynamic limit.

resulting saddle point root distributions $\rho_n^*(\lambda)$ can be obtained analytically [22]. The first few are given as

$$\rho_1^*(\lambda) = \frac{8(4+\lambda^2)}{\pi(19+3\lambda^2)(1+6\lambda^2+\lambda^4)} \tag{41}$$

$$\rho_2^*(\lambda) = \frac{8\lambda^2(9+\lambda^2)(4+3\lambda^2)}{\pi(2+\lambda^2)(16+14\lambda^2+\lambda^4)(256+132\lambda^2+9\lambda^4)} \tag{42}$$

$$\rho_3^* = \frac{8(1+\lambda^2)^2(5+\lambda^2)(16+\lambda^2)(21+\lambda^2)}{\pi(19+3\lambda^2)(9+624\lambda^2+262\lambda^4+32\lambda^6+\lambda^8)(509+5\lambda^2(26+\lambda^2))}. \tag{43}$$

## 5. Néel overlaps: Numerical results and overview

In this section we present the generic features of the overlaps between the Bethe states of the Heisenberg spin chain and the Néel state. We focus on finite chains of length up to $L \lesssim 40$. We consider the full Hilbert space of the chain, i.e., all the eigenstates. These are obtained from the Bethe ansatz approach. We exclude all the eigenstates corrsponding to BGT roots containing zero-momentum strings. The number of remaining eigenstates, that we denote as $\widetilde{Z}_{Neel}$ is given as a function of the chain size in terms of simple combinatorial formualas that we provide.

Interestingly, we demonstrate that for each finite chain the fraction of the eigenstates

with no zero-momentum strings is vanishing in the thermodynamic limit.
We restrict ourselves to eigenstates corresponding to BGT roots with no zero-momentum strings. As expected the Néel overlaps decay exponentially with the chain size in the thermodynamic limit.
Moreover, all the overlaps exhibit a vanishing behavior as a function of the eigenstate energy density, signalling that most of the Néel overlap is concentrated at low energies. We observe that the vast majority of eigenstates have negligible Néel overlap, as expected.
We show that only a small fraction of the eigenstates are relevant in the thermodynamic limit.
These are the Bethe states that are relevant in the quench action approach.
Finally, we focus on several overlap sum rules. As a consequence of the fact that we neglect the zero-momentum strings, we observe a striking violation of the sum rules for any finite chain. Specifically, all the sum rules exhibit vanishing behavior as $1/\sqrt{L}$ upon increasing the chain size, reflecting the vanishing of the fraction of the eigenstates with no zero-momentum strings.
Similarly, for the Majumdar-Ghosh state the sum rules vanish as $1/L$, again, reflecting the vanishing behaivor of the fraction of eigenstates with no zero-momentum strings.

### *5.1. Néel overlaps from the full scanning of the Hilbert space*

Here we present numerical results for the overlaps between the eigenstates of the Heisenberg spin chain and the Néel state. The data correspond to the full set of eigenstates with no zero-momentum strings and chain lengths $L \leq 38$. Their number $\widetilde{Z}_{Neel}$ is given as (see Appendix B for the proof)

$$\widetilde{Z}_{Neel} = B\Big(\frac{L}{2}, \frac{L}{4}\Big). \tag{44}$$

For $L = 38$ from (44) one has $\widetilde{Z}_{Neel} \sim 10^5$ eigenstates. Note that the total number of partiy-invariant eigenstates $Z_{Neel}$, which in principle give non-zero Néel overlap, is given as

$$Z_{Neel} = 2^{\frac{L}{2}-1} + \frac{1}{2}B\Big(\frac{L}{2}, \frac{L}{4}\Big) + 1. \tag{45}$$

The proof of (45) is reported in Appendix A.
We should stress that $Z_{Neel}$ provides only an upper bound for the number of eigenstates with non-zero Néel overlap (cf. for instance Table C1). This is due to the fact that parity-invariant eigenstates with a single even-length string with zero-momentum, which are counted in $Z_{Neel}$, have vanishing Néel overlap. This is due to the fact that in (26) the ratio of determinants is finite, whereas the prefactor (cf. (31)) vanishes if a single even-length string with zero momentum is present.
**Clarify what is the number/fraction of the even-length zero-momentum strings**

The results are obtained by generating all the parity-invariant BGT quantum numbers and using them to solve the BGT equations (12), obtaining the rapidities of the parity-invariant eigenstates of the $XXX$ chain. The overlaps with the Néel states are calculated numerically using (26).

Figure 1 plots the squared overlaps $|\langle\lambda|N\rangle|^2$ between the eigenstates $|\lambda\rangle$ of the $XXX$ chain and the Néel state $|N\rangle$ for chains with $L = 26, 32, 36, 38$. Figure 1 (a) shows the squared overlaps versus the eigenstate energy density $E/L$. Clearly, the overlaps decay exponentially as a function of $L$, as expected. Moreover, for each $L$ we observe a rapid decay as a function of the eigenstate energy density. This decay is exponential, as shown in the inset of Figure 1 (a).

Complementary information is shown in Figure 1 (b) plotting the the histograms of $-2\log|\langle\lambda|N\rangle|/L$ (overlap distribution function). Notice that $2\log|\langle\lambda|N\rangle|/L$ is the driving term in the Quench Action approach. The factor $1/L$ in the definition takes into account that all the overlaps vanish exponentially in the thermodynamic limit, or at least the overlaps that are relevant for the quench action. Notice that larger values of $-2\log|\langle\lambda|N\rangle|/L$, correspond to faster decaying, i.e., asymptotically for large $L$, smaller overlaps.

Figure 1 (b) demonstrates that the vast majority of the eigenstates have small Néel overlap. Specifically, a peak at $\sim 0.5$ is visible in the Figure, and a rapid decay at smaller values of ... .

Interestingly, the data suggest the behavior

$$|\langle\lambda|N\rangle|^2 \propto \exp(-\kappa L), \tag{46}$$

with $0.18 \lesssim \kappa \lesssim 0.7$. The vertical dash-dotted line in Figure 1 is the overlap between the ground state of the $XXX$ chain and the Néel state. This is obtained using the ground state root distribution $\rho_1(\lambda) \propto 1/\cosh(\pi\lambda)$ and (35). The dashed line denotes the Néel overlap $\sim 2/B(L, L/2)$ with the $S_z = 0$ component of the ferromagnetic state. The vertical dotted line in the Figure shows the expected result for $-2\log|\langle\lambda|N\rangle|/L$ in the thermodynamic limit as obtained from the quench action.

This is obtained by usigng (35) and the saddle point root distributions $\rho_n^*$ (cf. (41)-(43) for the results up to $n = 3$). Note that its position does not coincide with the peak of the overlap distribution function, as expected. This is reflecting the competition between the driving term and the entropy term in the quench action.

### *5.2. Néel overlap sum rules*

Here we investigate the effect of the Hilbert space truncation removed the zero-momentum strings on the Néel sum rules. We focus on the "trivial" sum rule, i.e., the normalization of the initial state

$$\langle N|N\rangle = \sum_{\lambda} |\langle\lambda|N\rangle|^2 = 1, \tag{47}$$

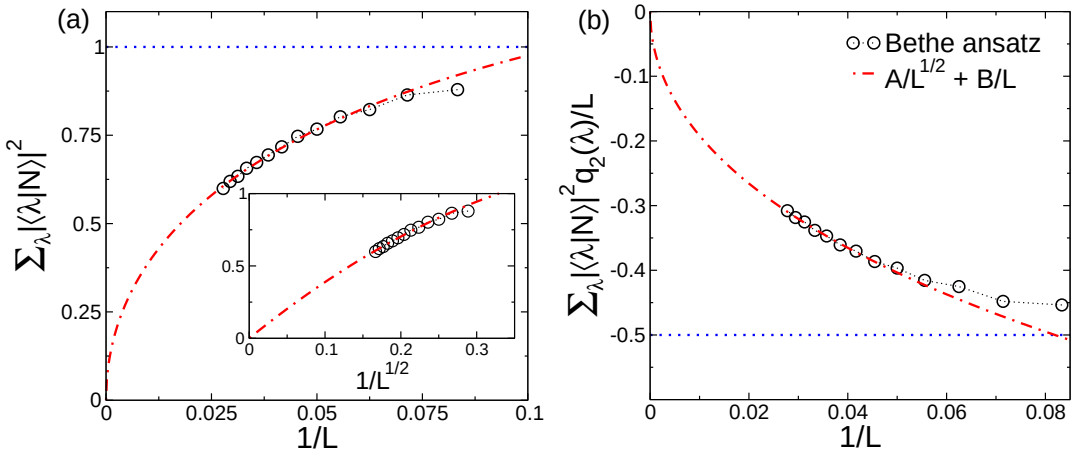


**Figure 2.** Overlap sum rules for the Neel state: The role of the zero-momentum strings. (a) The overlap sum rule $\sum_\lambda |\langle\lambda|N\rangle|^2 = 1$, with $|N\rangle$ the Neel state and $|\lambda\rangle$ the eigenstates of the $XXX$ spin chain. The $x$-axis shows $1/L$, with $L$ the chain length. The circles are Bethe ansatz results for chains up to $L = 36$. The results are obtained via a full scanning of the chain Hilbert space. Only the eigenstates with no zero-momentum strings are considered. The dash-dotted line is a fit to $A/L^{1/2} + B/L$, with $A, B$ fitting parameters. Inset: The same data as in the main Figure plotted versus $1/L^{1/2}$. (b) The same as in (a) for the sum rule $\sum_\lambda |\langle\lambda|N\rangle|^2 e(\lambda) = 1/2$, with $e(\lambda)$ the eigenstates energy density.

and the local conserved charges sum rules

$$Q_n^{(0)} = \langle N|Q_n|N\rangle = \sum_\lambda |\langle\lambda|N\rangle|^2 q_n(\lambda) \quad \text{with} \quad n \in \mathbb{N}, \tag{48}$$

where $Q_n$ are the conserved charges of the $XXX$ chain (cf. subsection 2.5) and $q_n(\lambda)$ are the charges eigenvalues over the generic Bethe state $|\lambda\rangle$ (cf. (22) and (23)).
In (48) $Q_n^{(0)}$ is the charge expectation value over the initial state, i.e., the Néel state. These can be calculated as done in Ref. [35].
Note that due to the locality of $Q_n$, the translational invariance of the initial state, and the periodic boundary conditions, the charge density $Q_n^{(0)}/L$ does not depend on the chain size. For the Néel state, in the thermodynamic limit $Q_n^{(0)}$ is obtained using (24) and the quench action root distributions $\boldsymbol{\rho}^*$ (cf. (41)-(43)).
The truncation of the chain Hilbert space removing the zero-momentum strings has dramatic effects on the sum rules (47) and (48).
This is illustrated in Figure 2 (a) focusing on the "trivial" sum rule (47) and in Figure 2 (b) for (48) with $n = 2$, i.e., the energy sum rule. For the Néel state, for any finite $L$ Eq. (**??**) gives $Q_2^{(0)}/L = -1/2$.
The circles in Figure 2 are the numerical results for the sum rules obtained via a full scanning of the Hilbert space of the Heisenberg chain, excluding the zero momentum strings. The data are plotted against the inverse chain length $1/L$, for $L \leq 38$. The expected results including all the eigenstates are shown as horizonthal dotted lines in the Figure.

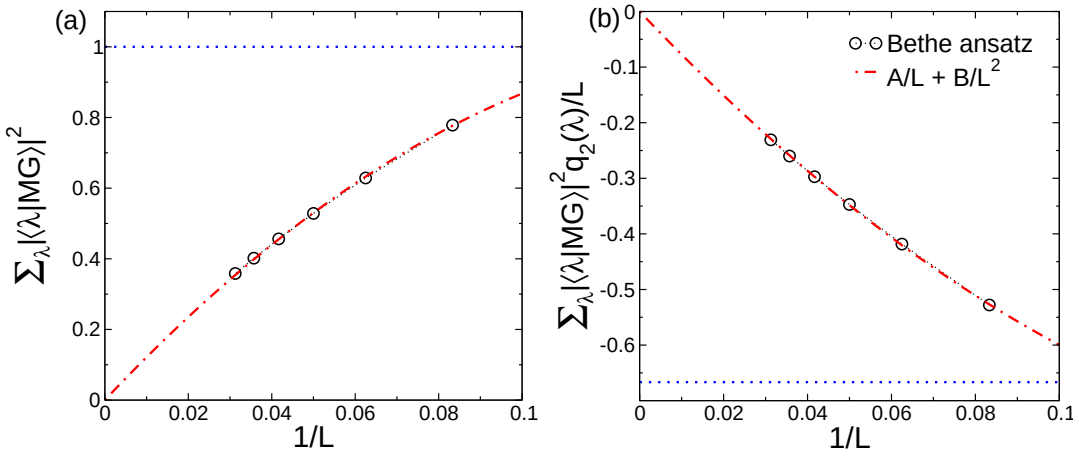


**Figure 3.** Overlap sum rules for the Majumdar-Ghosh (MG) state. (a) The overlap sum rule $\sum_\lambda |\langle\lambda|MG\rangle|^2 = 1$, with $|MG\rangle$ the Majumdar-Ghosh state and $|\lambda\rangle$ the eigenstates of the $XXX$ spin chain. The $x$-axis shows $1/L$, with $L$ the chain length. The circles are Bethe ansatz results for chains up to $L = 36$. The results are obtained via a full scanning of the chain Hilbert space. Only the eigenstates with no zero-momentum strings are considered. The dash-dotted line is a fit to $A/L + B/L^2$, with $A, B$ fitting parameters. (b) The same as in (a) for the sum rule $\sum_\lambda |\langle\lambda|MG\rangle|^2 e(\lambda) = 2/3$, with $e(\lambda) \equiv E/L$ the eigenstates energy density.

Clearly, both the sum rules are violated, due to the exclusion of the to zero-momentum strings. Moreover, in both panesl the data suggest a vanishing behavior upon increasing the chain size. In particular, the dash-dotted lines in the Figures are fits to $A/L^{1/2}+B/L$, with $A, B$ fitting parameters, which perfectly describes the behavior of the data.
The vanishing behavior as $\propto 1/L^{1/2}$ is reflecting the vanishing of the fraction of non-zero momentum string eigenstates in the thermodynamic limit. Precisely, from (45) and (44) one obtains

$$\frac{\widetilde{Z}_{Neel}}{Z_{Neel}} \propto \frac{4}{\sqrt{\pi L}}. \tag{49}$$

in the thermodynamic limit.
The asymptotic, i.e., at large $L$, behavior as $1/\sqrt{L}$ is not generic, meaning that it depends on the initial state $|\Psi_0\rangle$. This is illustrated in Figure 3, focusing on the Majumdar-Ghosh (MG) state. Panels (a) and (b) plot are the same as in Figure 2. The expected value for the energy density sum rule is $Q_2^{(0)} = -2/3$ (horizonthal dotted line in Figure 3). As for the Néel state only parity-invariant eigenstates containing no zero-momentum strings are consdidered. Note that their number $\widetilde{Z}_{MG}$ (cf. (B.7)) is now given as

$$\widetilde{Z}_{MG} = B\Big(\frac{L}{2}, \frac{L}{4}\Big) - B\Big(\frac{L}{2}, \frac{L}{4} - 1\Big). \tag{50}$$

Similar to Figure 2, due to the exclusion of the zero-momentum strings, the saturation rules exhibit vanishing behavior in the thermodynamic limit. However, in contrast with

the Néel case, one has the behavior $\sim 1/L$, as confirmed by the fits (dash-dotted lines in Figure 3).
Similar to the Néel case this reflects the same vanishing behavior of the eigenstates containing no zero-momentum strings $\widetilde{Z}_{MG}/Z_{MG}$ as

$$\frac{\widetilde{Z}_{MG}}{Z_{MG}} = \frac{4}{4+L}. \tag{51}$$

where $Z_{MG}$ is the total number of parity-invariant eigenstates having non-zero overlap with the Majumdar-Ghosh state.

## 6. Monte Carlo implementation of the quench action approach

In this section follwing Ref. [18] we present the implementation of the quench action approach, focusing on the $XXX$ chain. The key idea is to sample the eigenstates of the finite-size $XXX$ chain with the quench action probability distribution given in (39). Importantly, we restrict ourselves to the set of eigenstates of the $XXX$ chain with no zero-momentum strings. In subsection 6.1 we introduce the Monte Carlo algorithm. Using the Monte Carlo algorithm in subsection 6.2 we numerically demonstrates that the Néel sum rules (48) are recovered in the thermodynamic limit. The Hilbert space truncation is reflected in $\propto 1/L$ scaling corrections to the sum rules. Physically, this implies that despite the Hilbert space cut, the remaining eigenstates contain enough information to reproduce the correct physical behavior in the thermodynamic limit.
In the Bethe ansatz framework this means that the eigenstates sampled by the Monte Carlo method approach the quench action representative state in the thermodynamic limit. This is explicitly demonstrated here by numerically calculating the quench action root distributions $\boldsymbol{\rho}^*$, which are found in remarkable agreement with the analytical results.

### *6.1. Quench Action Monte Carlo algorithm*

The Monte Carlo procedure starts with a randomly selected parity-invariant eigenstate (Bethe state) of the $XXX$ chain in the sector with zero magnetization, i.e., $M = L/2$ particles.
Due to the fact that the Néel state is not invariant under $SU(2)$ rotations, to characterize the Bethe states one has to specify the number of infinite rapidities. Let us define the number of infinite rapidities $N_\infty$. Clearly, one has that the number of particles with finite rapidities $M'$ as $M' = L/2 - N_\infty$. The state is identified by a parity-invariant Bethe quantum number configuration $\mathcal{C}$. Due to the parity-invariance and the fact that zero-momentum strings are excluded, the state is characterized by the number $m'$ of parity-invariant rapidity pairs $\{\pm\lambda_j\}_{j=1}^{m'}$. The string content associated with the finite rapidity pairs is denoted as $\widetilde{\mathcal{S}} = \{\tilde{s}_1, \ldots, \tilde{s}_{m'}\}$. The Monte Carlo procedure generates a new parity-invariant eigenstate of the $XXX$ chain, and it consists of four steps as follows:

(1) Choose a new number of finite rapidities $M'_{new}$ and a parity-invariant rapidity pairs $m'_{new} \equiv M'_{new}/2$ with probability $\mathcal{P}(M'_{new})$ as

$$\mathcal{P}(M'_{new}) = \frac{\widetilde{Z}'_{Neel}(L, M'_{new})}{\widetilde{Z}_{Neel}(L)}, \tag{52}$$

where $\widetilde{Z}_{Neel}(L)$ is the total number of parity-invariant eigenstates with no zero-momentum strings (cf. (44)), and $\widetilde{Z}'_{Neel}$ is the number of parity invariant eigenstates with no zero-momentum strings in the sector with $M'_{new}$ particles with finite rapidities (cf. (B.6)).

(2) Choose a new a new string content $\widetilde{\mathcal{S}}' \equiv \{\tilde{s}'_1, \ldots, \tilde{s}_{m'_{new}}\}$ with probability $\mathcal{P}'(M'_{new}, \widetilde{\mathcal{S}}')$

$$\mathcal{P}'(M'_{new}, \widetilde{\mathcal{S}}') = \frac{1}{\widetilde{Z}'_{Neel}(L, M'_{new})} \prod_{n=1}^{m'_{new}} B\Big(\frac{L}{2} - \sum_{l=1}^{m'_{new}} t_{nl}\tilde{s}'_l, \tilde{s}'_n\Big), \tag{53}$$

where the matrix $t_{nl}$ is defined in (13).

(3) Generate a new parity-invariant quantum number configuration $\mathcal{C}'$ compatible with the $\widetilde{\mathcal{S}}'$ obtained in step (2). Solve the corresponding BGT equations (12), finding the rapidities $\{\pm\lambda'_j\}_{j=1}^{m'_{new}}$ of the new parity-invariant eigenstate.

(4) Calculate the overlap $\langle\{\lambda'_j\}_{j=1}^{m'_{new}}|N\rangle$ between the new eigenstate and the Néel state using (26) (29) (30) and (31). Accept the new eigenstate with the quench action Metropolis probability

$$\mathcal{P}''_{\lambda\to\lambda'} = \mathrm{Min}\Big\{1, \exp\Big(-2\Re(\mathcal{E}' - \mathcal{E})\Big)\Big\}, \tag{54}$$

where $\mathcal{E}' \equiv -\log\langle\{\lambda'_j\}_{j=1}^{m'_{new}}|N\rangle$, $\mathcal{E} \equiv -\log\langle\{\lambda_j\}_{j=1}^{m'_{new}}|N\rangle$, and $\Re$ denoting the real part.

Note that while the steps 1-3 generate the correct eigenstate energy density distribution, 4 weigh the different eigenstates with the quench action probability distribution.
For a generic observable $\mathcal{O}$, the long-time quench action value $\langle\mathcal{O}\rangle$ is obtained as the arithmetic average of the expectation value over the eigenstates $|\lambda\rangle$ sampled by the Monte Carlo as

$$\langle\mathcal{O}\rangle = \frac{1}{N_{mcs}}\sum_{\lambda}\langle\lambda|\mathcal{O}|\lambda\rangle, \tag{55}$$

with $N_{mcs}$ being the total number of Monte Carlo steps. Note that, as usual in Monte Carlo, some initial steps have to be neglected to ensure thermalization. Note that (55) applies to any observable $\mathcal{O}$ for which the the Bethe state expectation value $\langle\lambda|\mathcal{O}|\lambda\rangle$ (form factor) is known.

### *6.2. The Néel sum rules: Monte Carlo results*

The validity of the Monte Carlo approach for simulating the Quench-Action results is demonstrated in Figure 4. The Figure focuses on the Néel sum rules for the conserved

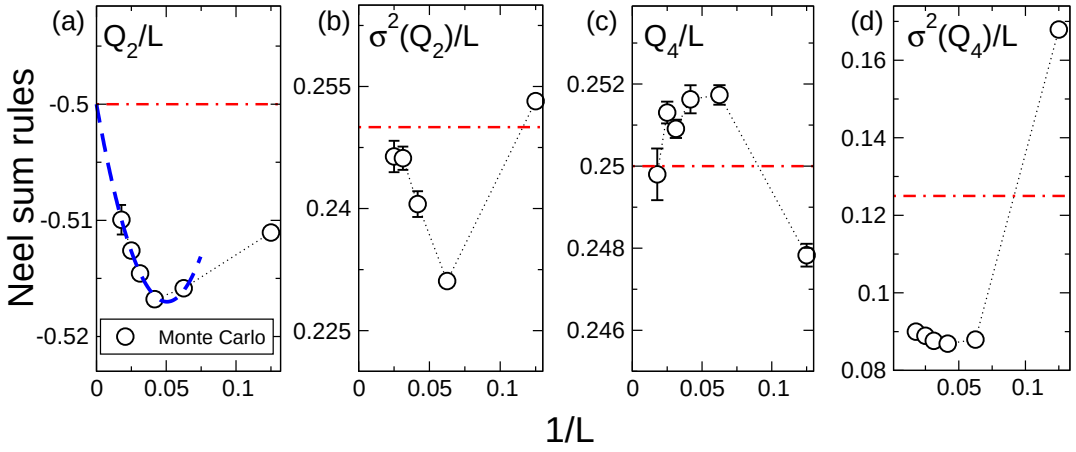


**Figure 4.** The overlap sum rules for the Neel state: Numerical results obtained using the Hilbert space Monte Carlo sampling approach. (a) The energy sum rule $\langle N|Q_2|N\rangle/L = -1/2$, with $Q_2/L$ the Hamiltonian density. We plot $\sum_\lambda |\langle\lambda|N\rangle|^2 Q_2(\lambda)/L = 1/2$, with $|\lambda\rangle$ the eigenstates of the $XXX$ chain, versus the inverse chain length $1/L$. The symbols are Monte Carlo data obtained by sampling the eigenstates of the $XXX$ chain. The dash-dotted line is the expected result. The dashed line is a fit to the behavior $-1/2 + A/L + B/L^2$, with $A, B$ fitting parameters. (b) The energy fluctuations sum rule $\sigma^2(Q_2)/L \equiv (\langle N|Q_2^2|N\rangle - \langle N|Q_2|N\rangle^2)/L = 1/4$. The horizontal line is the expected result. (c)(d) Same as in (a)(b) for the charge $Q_4$ and its fluctuations.

charges densities $Q_2/L$ and $Q_4/L$ (cf. subsection 2.5 and (48)) and their fluctuations $\sigma(Q_n)$, which are defined as

$$\sigma^2(Q_n) \equiv \langle N|Q_n^2|N\rangle - \langle N|Q_n|N\rangle^2 = \sum_\lambda |\langle N|\lambda\rangle|^2 q_n^2(\lambda) - \Big(\sum_\lambda |\langle N|\lambda\rangle|^2 q_n(\lambda)\Big)^2. \quad (56)$$

Panel (a) and (b) in Figure 4 show the sum rules for the energy density $Q_2/L$, and its density of fluctutations $\sigma^2(Q_2)/L$. It is straightforward to derive the Néel expectation value of the energy density fluctuations as $\sigma(Q_2)/L = 1/4$ (dash-dotted line in Figure 4 (b)).

The circles in the Figure are Monte Carlo data obtained using the procedure outlined in 6.1 for the Heisenberg spin chain with $L \leq 56$ sites. The data correspond to Monte Carlo simulations with $N_{mcs} \sim 10^7$ Monte Carlo steps (mcs). For the largest chain size $L = 56$ we used $N_{mcs} \sim$ .... The data are plotted versus inverse chain length $1/L$.

Interestingly, the Monte Carlo data strongly suggest that in the thermodynamic limit the sum rule saturates are restored, while violations are present for finite chains. This numerically demonstrates that the truncation of the Hilbert space, i.e., removing the zero-momentum strings, gives rise to scaling corrections, while the thermodynamic limit behavior is correctly reproduced. Furthermore, the data in panel (a) suggest the behavior $\propto 1/L$ for the scaling corrections, as confirmed by the fit to $-1/2 + A/L + b/L^2$ (dashed line in the Figure), with $A, B$ fitting parameters.

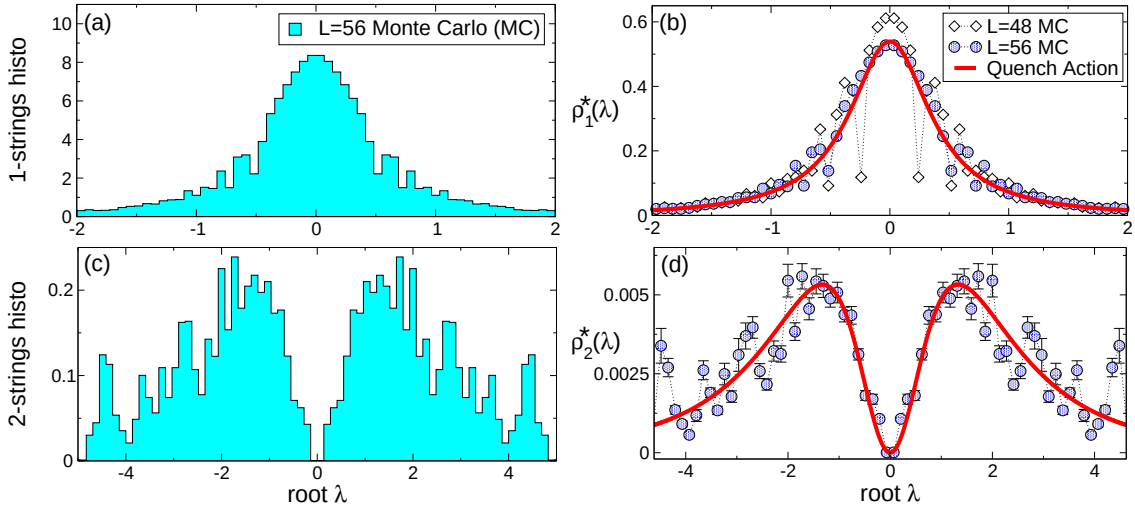


**Figure 5.** The Quench-Action steady state root ddistributions $\rho_1(x)$ and $\rho_2(x)$: Monte Carlos results. (a) The histograms of the 1-string rapidities sampled in the Monte Carlo. The $x$-axis shows the 1-string BGT root $\lambda$. The data are for a chain with $L = 56$ sites and $N_{mcs} \sim 10^7$ Monte Carlo steps. The data are divided by a factor $10^6$ for plotting convenience. The width of the histogram bin is $\Delta\lambda \sim 0.07$. (b) The same as in (a) for the 2-string roots sampled in the Monte Carlo. (b) The extracted 1-string root distribution $\rho_1(\lambda)$ plotted versus $\lambda$ for two chains with $L = 48$ and $L = 56$ (diamond and circles, respectively). The full line is the Quench-Action analytic result in the thermodynamic limit. (d) The same as in (c) for the 2-string root density $\rho_2(\lambda)$. In both (c)(d) the oscillations are finite-size effects, whereas the error bars show the statistical Monte Carlo error.

The same behavior should be expected for the energy fluctuations $\sigma^2(Q_2)$, although this is difficult to extract numerically due to the large Monte Carlo error bar.

Finally, panels (c) and (d) in Figure 4 are the same as (a)(b), but for the charge $Q_4$. While for $Q_4/L$ the Monte Carlo result for $L = 48$ is already compatible with the expected result $Q_4/L = 1/4$ in the thermodynamic limit, the scaling corrections of the fluctuations $\sigma^2(Q_4)$ are larger, and the Monte Carlo data show significant deviations from the thermodynamic limit up to $L = 56$.

This is explained that the support of $Q_4$, i.e., the number of sites where the operator acts non trivially is larger than for $Q_2$ (see [36] for the precise expression), and it is natural to assume that scaling corrections increase upon increasing the support of the operator considered.

### *6.3. The quench action root distributions*

The BGT root distributions corresponding to the quench action steady state (cf. (41)-(43)) $\boldsymbol{\rho} = \{\rho_n(\lambda)\}_{n=1}^{\infty}$ can be extracted from the Monte Carlo simulation. This has been shown in Ref. [18] for the GGE representative state.

The underlying idea is that for the local observables considered in this work the

eigenstate expectation value $\langle\lambda|\mathcal{O}|\lambda\rangle$ entering in (55) becomes

$$\langle\lambda|\mathcal{O}|\lambda\rangle = \sum_{n,\gamma} \mathcal{O}(\lambda_{n;\gamma}), \tag{57}$$

with the set of solutions of the BGT equations $\{\lambda_{n;\gamma}\}$ identifying the Bethe state $|\lambda\rangle$. By comparing (55) and ... one obtains

$$\frac{1}{N_{mcs}} \sum_{\{\lambda_{n;\gamma}\}} \mathcal{O}_n(\lambda_{n;\gamma}) \to \int_{-\infty}^{+\infty} d\lambda \rho_n(\lambda)\mathcal{O}_n(\lambda). \tag{58}$$

This suggests that for any $n$ the histograms of the BGT roots corresponding to the $n$-strings sampled in the Monte Carlo should converge in the thermdynamic limit to the root distribution $\rho_n$.

This is demonstrated numerically in Figure 5 for the first two root distributions $\rho_1^*(\lambda)$ (panel (a)(b)) and $\rho_2^*(\lambda)$ (panel (c)(d)). The data are obtained using the algorithm described in subsection 6.1 for chains with up to $L \leq 56$ sites. The data for $L = 48$ correspond to a Monte Carlo history with $N_{mcs} \sim 10^7$ Monte Carlo steps (cf. (55)), whereas we used $N_{mcs} \sim 10^8$ for $L = 56$.

Panel (a) and (c) show the histograms of the 1-string and 2-string BGT roots sampled in the Monte Carlo, respectively for the chain with $L = 56$ sites. The $y$-axis is divided by a factor $10^6$ for convenience. The width of the histogram bins $\Delta\lambda$ is $\Delta\lambda \approx 0.02$ and $\Delta\lambda \approx 0.001$ for $\rho_1(\lambda)$ and $\rho_2(\lambda)$, respectively. The histogram fluctuations are due both to the finite statistics (finite $N_{mcs}$) and to the finite size of the chain.

The extracted quench action saddle point root distributions $\rho_1^*(\lambda)$ and $\rho^*(\lambda)$ are shown in panels (b) and (d). The data are the same as in panel (a)(c). The normalization of the histograms is chosen such as to match the analytical results from (41) and (42), i.e., $\int d\lambda \rho_1^*(\lambda) \approx 0.31$ and $\int d\lambda \rho_2^*(\lambda) \approx 0.015$. The Monte Carlo error bars shown in the Figure are obtained with a standard jackknife analysis [37, 38]. The continuous lines are the expected analytic result in the thermodynamic limit given in (41) and (42). Clearly, $\rho_1(\lambda)$ is in good agreement with the Monte Carlo data in the whole range $-2 \leq \lambda \leq 2$ considered. The statistical error bars are smaller than the symbol size. The oscillations are due to the finite size of the chain, and decrease with the chain size (see the data for $L = 48$). On the other hand, larger (oscillating) finite size effects are observed for $\rho_2(\lambda)$. These deviations are larger on the tails of the root distribution. This is expected since large $\lambda$ correspond to large quasimomenta, which are more sensitive to the finite size of the chain. Moreover, the Monte Carlo error bars are clearly visible. This is due to the fact that since $\int d\lambda \rho_2^*(\lambda)/\sum_n \int d\lambda \rho_n^*(\lambda) \approx 0.04$, the statistics available to estimate $\rho_2^*(\lambda)$ is effectively reduced as compared to $\rho_1^*(\lambda)$. Finally, we numerically checked that this effect is more dramatic for the longer strings root distribution, and larger statistics and larger chain would be needed already to extract $\rho_3(\lambda)$

## 7. Conclusions

We presented a Monte Carlo implementation of the quench action method for integrable spin chains. We focused on the spin-1/2 isotropic Heisenberg spin chain ($XXX$ chain) and the quench from the zero-momentum Néel state. The approach extends the Monte Carlo approach developed in Ref. [18] to simulate the Generalized Gibbs Ensemble in integrable models. The key idea of the approach is the Monte Carlo sampling of the model Hilbert space with the quench action, equivalently the Diagonal Ensemble, probability distribution given in (2).

The approach is based on the knowledge of the overlaps between the pre-quench Néel state $|N\rangle$ and the eigenstates of the model that have been obtained recently [29, 22, 33, 24, 23, 39].

Besides the overlaps the method is based on the knowledge of the Hilbert space structure provided by the Bethe ansatz formalism and on the Bethe-Gaudin-Takahashi (BGT) equations. The approach is devised for finite-size systems. Thermodynamic quantities can be extracted using finite-size scaling.

We first focused on the importance of the so-called zero-momentum strings. These corresponds to components of the Bethe wavefunctions corresponding to bound states of many down spins (strings in the Bethe ansatz language) with zero center of mass momentum. These are usually neglected in the quench action approach [22]. The reason is that zero momentum strings leads to singularities in the overlap formulas, which make extracting the thermodynamic limit tricky. Moreover, it is argued that zero-momentum strings give rise only to scaling corrections to the quench action results, which are unimportant in the thermodynamic limit.

Importantly, one should observe that for a finite chain the vast majority of eigenstates contain zero-momentum strings. More precisely, for the quench from the Néel state the fraction of eigenstates with no zero-momentum strings vanish as $\propto L^{-1/2}$.

Moreover, the only eigenstates having non zero Néel overlaps (and non zero overlap with the Majumdhar-Ghosh state) are the so-called parity invariant eigenstates. The total number of parity-invariant eigenstates of the Heisenberg spin chain is given in terms of the chain length by a simple combinatorial formula that we provide. We provide similar combinatorial formulas for the total number of parity-invariant eigenstates at fixed number of down spins and fixed string content, i.e., the number of many-spin bound states present in each eigenstates.

In order to understand the importance of the zero-momentum strings we calculated the overlap distribution function including all the eigenstates of the chain for chains up to $L = 38$ sites. We excluded the zero-momentum strings.

We focused on some exact sum rules for the local integrals of motion of the $XXX$ chain. Strikingly, the exclusion of the zero momentum strings gives rise to violations of the sum rules. Precisely, we numerically observe that the sum rules exhibit the vanishing behavior $\propto L^{-\frac{1}{2}}$, which reflects the vanishing of the fraction of eigenstates with no zero-momentum strings.

The behavior $\propto L^{-\frac{1}{2}}$ is not generic, but it depends on the pre-quench initial state. We demonstrated that by considering the quench from the Majumdar-Ghosh state. We observed that the sum rule vanish as $1/L$, again reflecting the vanishing as $1/L$ of the fraction of eigenstates with no zero-momentum strings.

We observed that the vast majority of the eigenstates have neglegible overlap with the Néel state. This implies that the eigenstates relevant for the quench action are a small fraction of the total number of eingestates having in principle non-zero Néel overlap.

Next we presented a Monte Carlo implementation of the quench action method. This is obtained by resampling with the quench action probability measure the Hilbert space of the $XXX$ chain, restricted to the sector of the Hilbert space with no zero-momentum strings.

This is obtained using a standard Metropolis algorithm. Importantly, we numerically demonstrated that the only consequence of the Hilbert space restriction to strings with finite momentum are scaling corrections $1/L$ to physical observables.

Specifically, we focused on the sum rules for the local conserved quantities of the $XXX$ chain. We numerically observed that, although for finite chains violations of the sum rules are present, these violations decay upon increasing the chain size, and the sum rules are restored in the thermodynamic limit.

Finally, we extracted from the Monte Carlo the BGT root distributions characterizing the quench action saddle point. These are obtained from the BGT roots identifying the $XXX$ chain eigenstates sampled in the Monte Carlo. We observed that, although the finite size gives rise to oscillating scaling corrections, already for relatively small chains with $L = 56$ sites, the first BGT root distribution $\rho_1^*(\lambda)$ is in impressive agreement with the analytic result in the thermodynamic limit.

## Appendix A. Eigenstates with nonzero Néel overlap: eigenstates counting and string content

Here we prove that the total number of eigenstates with Néel nozero overlap $Z_{Neel}(L)$for a chain of length $L$ is given as

$$Z_{Neel} = 2^{\frac{L}{2}-1} + \frac{1}{2}B\Big(\frac{L}{2}, \frac{L}{4}\Big) + 1. \tag{A.1}$$

For simplicity here we restrict ourselves to the situation with $L$ divisible by four. The strategy to prove (A.1) is to count all the possible parity-invariant BGT quantum numbers configurations. Let us consider the sector with fixed number of particles $M$, and a generic string content $\mathcal{S} = \{s_1, s_2, \ldots, s_M\}$. Here $s_n$ is the number of $n$-strings, and one has the constraint $\sum_k k s_k = M$.

It is straightforward to check that total number of parity-invariant quantum number pairs $\mathcal{N}_n(L, \mathcal{S})$ in the $n$-string sector is given as

$$\mathcal{N}_n(L, \mathcal{S}) = \Big\lfloor \frac{L}{2} - \frac{1}{2}\sum_{m=1}^{M} t_{nm} s_m \Big\rfloor. \tag{A.2}$$

where $t_{nm} \equiv 2\text{Min}(n,m) - \delta_{n,m}$. The number of parity-invariant quantum number configurations (i.e., eigenstates) $\mathcal{N}(L,\mathcal{S})$ compatible with string content $\mathcal{S}$ is obtained by choosing in all the possible ways the parity-invariant quantum number pairs independently in each $n$-string sector, which implies that

$$\mathcal{N}(L,\mathcal{S}) = \prod_{m=1}^{M} B\left(\mathcal{N}_m, \left\lfloor \frac{s_m}{2} \right\rfloor\right). \tag{A.3}$$

Here the product is because each string sector is treated independently, while the factor $1/2$ in $s_m/2$ is because since all quantum numbers are organized in pairs, only half of the quantum numbers have to be specified. Note that in each $n$-string sector only one zero momentum (i.e., zero quantum number) string is allowed, due to the Pauli principle. Moreover, $s_m$ is odd (even) only if the zero momentum string is (not) present. The floor function $\lfloor\cdot\rfloor$ in (A.3) reflects that the quantum number of zero-momentum strings is fixed.

We now consider the string configurations with particle number $0 \leq \ell \leq M$ and fixed number of strings $1 \leq q \leq M/2$. Note that the maximul allowed string length is $M/2$ beacause of parity invariance. Note also that in determining $q$ strings of different length are treated equally. Clearly, one has that $\sum_m s_m = q$. For a given fixed pair $\ell, q$ the total number of quantum number configurations is given as

$$\mathcal{N}'(L,\ell,q) = \sum_{\{\{s_m\}:\sum m s_m=\ell,\sum s_m=q\}} \mathcal{N}(L,\mathcal{S}), \tag{A.4}$$

where the sum is over the content $\{s_m\}_{m=1}^M$ compatible with the constraints $\sum_m s_m = q$ and $\sum_m m s_m = \ell$. The strategy is to write a recursive relation for $\mathcal{N}'(L,\ell,q)$. To this purpose it is useful to consider the shifted string content $\mathcal{S}'$ defined as

$$\mathcal{S}' \equiv \{s_{m+1}\} \quad \text{with } s_m \in \mathcal{S},\ \forall m. \tag{A.5}$$

Using the definition of $t_{ij}$, it is straightforward to derive that

$$t_{ij} = t_{i-1,j-1} + 2, \tag{A.6}$$

which implies that $\mathcal{N}_n(L,\mathcal{S})$ (see (A.2)) satisfies the recursive equation

$$\mathcal{N}_n(L,\mathcal{S}) = \mathcal{N}_{n-1}(L-2q,\mathcal{S}'). \tag{A.7}$$

After substituting in (A.3) one obtains

$$\mathcal{N}(L,\mathcal{S}) = B\Big(\mathcal{N}_1(L,\mathcal{S}), \left\lfloor \frac{s_1}{2} \right\rfloor\Big)\mathcal{N}(L-2q,\mathcal{S}'). \tag{A.8}$$

Finally, after substituting (A.8) in (A.4), one obtains a recursive relation for $\mathcal{N}'(L,\ell,q)$ as

$$\mathcal{N}'(L,\ell,q) = \sum_{s=0}^{q-1} B\Big(\frac{L}{2} - q + \left\lfloor \frac{s}{2} \right\rfloor, \left\lfloor \frac{s}{2} \right\rfloor\Big)\mathcal{N}'\left(L-2q, \ell-q, q-s\right), \tag{A.9}$$

with the constraint that when $\ell = q$ one has

$$\mathcal{N}'(L,q,q) = B\Big(\left\lfloor \frac{L-q}{2} \right\rfloor, \left\lfloor \frac{q}{2} \right\rfloor\Big). \tag{A.10}$$

This is obtained by observing that if $\ell = q$ only 1-strings are allowed and (A.2) gives $\mathcal{N}_n(L, \mathcal{S}) = \lfloor (L-q)/2 \rfloor$.
It is straightforward to check that for even $q$ the ansatz

$$\mathcal{N}'(L, \ell, q) = \frac{q}{\ell} B\Big(\frac{L-\ell}{2}, \frac{q}{2}\Big) B\Big(\frac{\ell}{2}, \frac{q}{2}\Big), \tag{A.11}$$

satisfies (A.9). For odd $q$ the solution of (A.9) is

$$\mathcal{N}'(L, \ell, q) = \frac{\ell - q + 1}{\ell} B\Big(\frac{L-\ell}{2}, \frac{q-1}{2}\Big) B\Big(\frac{\ell}{2}, \frac{q-1}{2}\Big). \tag{A.12}$$

The number of eigenstates in the sector with $\ell$ particles with nonzero Néel overlap $Z'_{Neel}(L, \ell)$ are obtained by summing over all possible values of $q$ as

$$Z'_{Neel}(L, \ell) = \sum_{q=1}^{\ell} \mathcal{N}'(L, \ell, q). \tag{A.13}$$

It is convenient to split the summation in (A.13) considering odd values of $q$ and even $q$ separately. For odd $q$ one obtains

$$\sum_{k=0}^{\ell/2-1} \mathcal{N}'(L, \ell, 2k+1) = B\Big(\frac{L}{2} - 1, \frac{\ell}{2} - 1\Big), \tag{A.14}$$

while for even $q$ one has

$$\sum_{k=0}^{\ell/2} \mathcal{N}'(L, \ell, 2k) = B\Big(\frac{L}{2} - 1, \frac{\ell}{2}\Big). \tag{A.15}$$

Putting everything together one obtains

$$Z'_{Neel}(L, \ell) = B\Big(\frac{L}{2} - 1, \frac{\ell}{2} - 1\Big) + B\Big(\frac{L}{2} - 1, \frac{\ell}{2}\Big). \tag{A.16}$$

The total number of eigenstates with nonzero Néel overlap $Z_{Neel}(L)$ (cf. (A.1)) is obtained from (A.16) by summing over the allowed values of $\ell = 2k$ with $k = 0, 1, \ldots, \ell/2$.
Note that the total number $Z_{MG}$ of parity-invariant eigenstates having non zero overlap with the Majumdar-Ghosh state is obtained from Eq (A.16) replacing $\ell = L/2$, to obtain

$$Z_{MG} = B\Big(\frac{L}{2} - 1, \frac{L}{4} - 1\Big) + B\Big(\frac{L}{2} - 1, \frac{L}{4}\Big). \tag{A.17}$$

Physically, this is due to the fact that the Majumdar-Ghosh state is invariant under $SU(2)$ rotations, which implies that only eigenstates with zero total spin $S = 0$ can have non zero overlap.

## Appendix B. Excluding the zero-momentum strings

Here we demonstrate that the total number of eigenstates with nonzero Néel overlap, which do not contain zero-momentum strings, $\widetilde{Z}_{Neel}(L)$ is given as

$$\widetilde{Z}_{Neel}(L) = B\Big(\frac{L}{2}, \frac{L}{4}\Big). \tag{B.1}$$

Given a generic $M$-particle eigenstate of the $XXX$ chain, due to parity invariance, if one excludes the zero-momentum strings only $n$-strings with length $n \leq M/2$ are allowed. Similarly, the string content is of the form $\widetilde{\mathcal{S}} \equiv \{\tilde{s}_1, \ldots, \tilde{s}_{M/2}\}$, i.e., $\tilde{s}_m = 0 \; \forall m > M/2$. Note that due to parity invariance and to the exclusion of the zero-momentum strings one has that $\tilde{s}_m$ is always an even integer. Clearly one has $\sum_{m=1}^{M/2} m\tilde{s}_m = M$.
The total number of parity-invariant quantum numbers $\widetilde{\mathcal{N}}_n$ in the $n$-string sector is given as

$$\widetilde{\mathcal{N}}_n(L, \widetilde{\mathcal{S}}) = \frac{L}{2} - \frac{1}{2}\sum_{m=1}^{M/2} t_{nm}\tilde{s}_m. \tag{B.2}$$

The proof now proceeds as in Appendix A. One can define the total number of eigenstates with nonzero Néel overla in the sector with $\ell$ particles and $q$ different strings as $\widetilde{\mathcal{N}}'(L, \ell, q)$. Note that due to parity invariance and the exclusion of zero-momentum strings, $q$ must be even. It is straigtforward to show that $\widetilde{\mathcal{N}}'(L, \ell, q)$ obeys the recursive relation

$$\widetilde{\mathcal{N}}'(L, \ell, q) = \sum_{s=0}^{q/2-1} B\Big(\frac{L}{2} - q + s, s\Big)\widetilde{\mathcal{N}}'\Big(L - 2q, \frac{\ell - q}{2}, \frac{q}{2} - s\Big), \tag{B.3}$$

with the constraint

$$\widetilde{\mathcal{N}}'(L, 1, 1) = \frac{L}{2} - 1. \tag{B.4}$$

It is straightforward to check that the solution of (B.3) is given as

$$\widetilde{\mathcal{N}}'(L, \ell, q) = \frac{L - 2\ell + 2}{L - \ell + 2} B\Big(\frac{L - \ell}{2} + 1, q\Big) B\Big(\frac{\ell}{2} - 1, \frac{q}{2} - 1\Big). \tag{B.5}$$

After summing over the allowed values of $q = 2k$ with $k = 1, 2, \ldots, \ell/2$ one obtains the total number of eigenstaets with nonzero Néel overlap at fixed number of particles $\ell$ $\widetilde{Z}'_{Neel}(L, \ell)$ as

$$\widetilde{Z}'_{Neel}(L, \ell) = B\Big(\frac{L}{2}, \frac{\ell}{2}\Big) - B\Big(\frac{L}{2}, \frac{\ell}{2} - 1\Big). \tag{B.6}$$

Summing over $\ell$ one obtains (**??**). Similar to (A.17) the total number of eigenstates $\widetilde{Z}_{MG}$ with no zero-momentum strings having non-zero overlap with the Majumdar-Ghosh state is obtained from (B.6) replacing $\ell \to L/2$, to obtain

$$\widetilde{Z}_{MG} = B\Big(\frac{L}{2}, \frac{L}{4}\Big) - B\Big(\frac{L}{2}, \frac{L}{4} - 1\Big). \tag{B.7}$$

Interestingly, using (A.17) and (B.7), one obtains that the ratio $\widetilde{Z}_{MG}/Z_{MG}$ is given as

$$\frac{\widetilde{Z}_{MG}}{Z_{MG}} = \frac{4}{4 + L}. \tag{B.8}$$

## Appendix C. Exact Néel and Majumdar-Ghosh overlaps for a small Heisenberg chain

In this section we provide exact diagonalization results for the overlap of both the Néel state and the Majumdar-Ghosh (MG) state with all the eigenstates of the Heisenberg spin chain with $L = 12$ sites. We also provide the corresponding results obtained using the string hypothesis and the overlap formulas (26) and (33), restricting ourselves to eigenstates with no zero-momentum strings.

### *Appendix C.1. Néel overlap*

The overlaps between all the eigenstates of the Heisenberg spin chain and the Néel state are reported in Table C1. The first column in the Table shows the string content $\mathcal{S} \equiv \{s_1, \ldots, s_M\}$, with $M$ being the number of finite rapidities. The number of infinite rapidities $N_\infty = L/2 - M$ is also reported. Note that eigenstates containing infinite rapidities correspond to different $S_z$ eigenvalue. The second column shows $2I_n^+$, with $I_n$ the Bethe-Gaudin-Takahashi quantum number identifying the BGT rapidity of the $n$-string. Due to the parity invariance only the positive quantum numbers are reported. The total number of independent strings, i.e., $q \equiv \sum_j s_j$, is reported in the third column. The fourth column is the eigenstate's energy eigenvalue $E$. The last two columns show the squared Néel overlaps and the corresponding result obtained using the Bethe-Gaudin-Takahashi equations, respectively. In the last column only the case with no zero-momentum strings is considered. The deviations from the exact diagonalization results (digits with different colors) have to be attributed to the string hypothesis. Notice that the overlap between the Néel state and the $S_z = 0$ eigenstate in the sector with maximal total spin $S = L/2$ (first column in Table C1), is given analytically as $2/B(L, L/2)$, with $B(x, y)$ the Newton binomial.

Figure C1 plots the squared overlaps $|\langle\lambda|N\rangle|^2$ between the Néel state and the eigenstates of the chain. The overlaps are plotted against the eigenstate energy density $E/L \in [-\log(2), 0]$. The circles are exact diagonalization results for all the chain eigenstates (382 eigenstates), whereas the crosses denote the overlaps calculated using formula (26), and the Bethe-Gaudin-Takahashi equations. Note that only the eigenstates with no zero-momentum strings are shown (252 eigenstates) in the Figure. Panel (a) in the Figure is an overview of all the results. Panels (b)-(d) correspond to zooming to the smaller overlap values $|\langle N|\lambda\rangle| \lesssim 0.02$, $|\langle N|\lambda\rangle| \lesssim 0.002$, and $|\langle N|\lambda\rangle| \lesssim 10^{-5}$.

Clearly, the overlaps decay rapidly upon increasing the energy density. This is expected since the $XXX$ Hamiltonian expectation value over the Néel state is $\langle N|H|N\rangle = -1/2$. Importantly, the agreement between the exact diagonalization results and the results obtained using the BGT equations (**??**) is excellent, confirming the validity of the string hypothesis.

Bethe states with nonzero Néel overlap ($L = 12$)

| String content | $2I_n^+$ | $q$ | E | $\|\langle\lambda\|N\rangle\|^2$ (exact) | $\|\langle\lambda\|N\rangle\|^2$ (BGT) |
|---|---|---|---|---|---|
| 6 inf | - | - | 0 | 0.002164502165 | 0.002164502165 |
| {2,0} 4 inf | $1_1$ | 2 | −3.918985947229 | 0.096183409244 | 0.096183409244 |
| | $3_1$ | | −3.309721467891 | 0.011288497947 | 0.011288497947 |
| | $5_1$ | | −2.284629676547 | 0.004542580506 | 0.004542580506 |
| | $7_1$ | | −1.169169973996 | 0.002752622983 | 0.002752622983 |
| | $9_1$ | | −0.317492934338 | 0.002116006203 | 0.002116006203 |
| {4,0,0,0} 2 inf | $1_13_1$ | 4 | −7.070529325964 | 0.310133033838 | 0.310133033838 |
| | $1_15_1$ | | −5.847128730477 | 0.129277023687 | 0.129277023687 |
| | $1_17_1$ | | −4.570746557876 | 0.085992436024 | 0.085992436024 |
| | $3_15_1$ | | −5.153853093221 | 0.015256395523 | 0.015256395523 |
| | $3_17_1$ | | −3.916336243695 | 0.010091113504 | 0.010091113504 |
| | $5_17_1$ | | −2.817696043731 | 0.004059780228 | 0.004059780228 |
| {0,2,0,0} 2 inf | $1_2$ | 2 | −1.905667167442 | 0.001207238321 | 0.001207245406 |
| | $3_2$ | | −1.368837200825 | 0.002340453815 | 0.002325724713 |
| | $5_2$ | | −0.681173793635 | 0.001921010489 | 0.001939001396 |
| {1,0,1,0} 2 inf | $0_10_3$ | 2 | −2.668031843135 | 0.034959609810 | - |
| {6,0,0,0,0,0} 0 inf | $1_13_15_1$ | 6 | −8.387390917445 | 0.153412152966 | 0.153412152966 |
| {2,2,0,0,0,0} 0 inf | $1_11_2$ | 4 | −5.401838225870 | 0.040162686361 | 0.041042488913 |
| | $3_11_2$ | | −4.613929948329 | 0.004636541934 | 0.004730512604 |
| | $5_11_2$ | | −3.147465758841 | 0.001335522556 | 0.001337334035 |
| {3,0,1,0,0,0} 0 inf | $0_12_10_3$ | 4 | −6.340207488736 | 0.052743525774 | - |
| | $0_14_10_3$ | | −5.203653009936 | 0.015022005621 | - |
| | $0_16_10_3$ | | −3.788693957250 | 0.011144489334 | - |
| {1,0,0,0,1,0} 0 inf | $0_10_5$ | 2 | −2.444293750583 | 0.005887902992 | - |
| {0,0,2,0,0,0} 0 inf | $1_3$ | 2 | −1.111855930538 | 0.001342476001 | 0.001384980817 |
| {0,1,0,1,0,0} 0 inf | $0_20_4$ | 2 | −1.560671012472 | 0.000026982174 | - |

**Table C1.** All Bethe states for $L = 12$ having nonzero overlap with the zero-momentum Néel state. The first column shows the string content of the Bethe states, including the number of infinite rapidities. The second and third column show $2I_n^+$, with $I_n^+$ the BGT quantum numbers identifying the different states, and the number $q$ of independent strings. In the second column only the positive BGT numbers are shown. The fourth column is the Bethe state eigenenergy. Finally, the last two columns show the exact overlap with the Néel state and the approximate result obatained using the BGT equations. In the last column Bethe states containing zero-momentum strings are excluded. Deviations from the exact result (digits with different colors) are attributed to the string hypothesis.

### *Appendix C.2. Majumdar-Ghosh overlap*

The overlap between the Heisenberg chain eigenstates with the Majumdar-Ghosh state are shown in Table C2. The conventions on the representation of the eigenstates is the same as in Table C1. Note that in contrast with the Néel state, only the eigenstates with zero total spin $S = 0$ have non zero overlap, i.e., no eigenstates with infinite rapidities are present, which reflect that the Majumdar-Ghosh state is unvariant under $SU(2)$ rotations.

[1] I. Bloch, J. Dalibard, and W. Zwerger, Rev. Mod. Phys. **80**, 885 (2008).
[2] M. Greiner, O. Mandel, T. Hänsch, and I. Bloch, Nature (London) **419**, 51 (2002).
[3] T. Kinoshita, T. Wenger, and D. S. Weiss, Nature (London) **440**, 900 (2008).
[4] S. Hofferberth, I. Lesanovsky, B. Fischer, T. Schumm, and J. Schiedmayer, Nature (London) **449**,

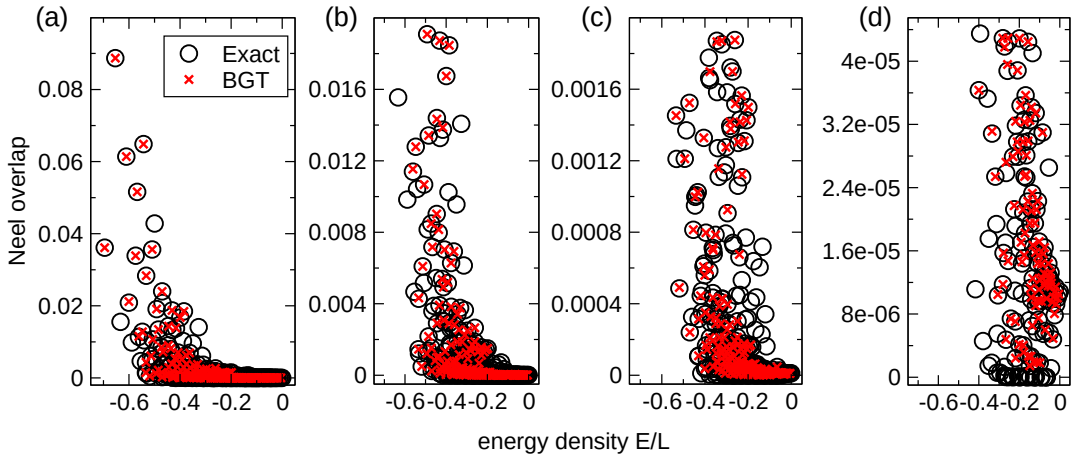


**Figure C1.** The squared overlap $|\langle N|\lambda\rangle|^2$ between the the Neel state $|N\rangle$ and the eigenstates $|\lambda\rangle$ of the $XXX$ chain with $L = 20$ sites. Only non-zero overlaps are shown. In all the panels the $x$-axis shows the eigenstate energy density $E/L$. The circles are the exact diagonalization results for all the non-zero overlaps. The crosses are the Bethe ansatz results obtained using the Bethe-Gaudin-Takahashi equations. The missing crosses correspond to eigenstates containing zero-momentum strings. (a) Overview of all the non-zero overlaps. (b)(c)(d) The same overlaps as in (a) zooming in the regions $[0, 0.2]$, $[0, 0.020]$, and $[0, 4 \cdot 10^{-5}]$. The discrepancies between the ED and the Bethe ansatz results are attributed to the string deviations.

Bethe states with nonzero Néel overlap ($L = 12$)

| String content | $2I_n^+$ | $q$ | E | $\lvert\langle\lambda\rvert MG\rangle\rvert^2$ (exact) | $\lvert\langle\lambda\rvert MG\rangle\rvert^2$ (BGT) |
|---|---|---|---|---|---|
| {6,0,0,0,0,0} | $1_1 3_1 5_1$ | 6 | −8.387390917445 | 0.716615769224 | 0.716615769224 |
| {2,2,0,0,0,0} | $1_1 1_2$ | 4 | −5.401838225870 | 0.055624700196 | 0.054033366543 |
| | $3_1 1_2$ | | −4.613929948329 | 0.005687428810 | 0.005582983043 |
| | $5_1 1_2$ | | −3.147465758841 | 0.002107475934 | 0.002107086933 |
| {3,0,1,0,0,0} | $0_1 2_1 0_3$ | 4 | −6.340207488736 | 0.205891158647 | - |
| | $0_1 4_1 0_3$ | | −5.203653009936 | 0.038832154450 | - |
| | $0_1 6_1 0_3$ | | −3.788693957250 | 0.006019410923 | - |
| {1,0,0,0,1,0} | $0_1 0_5$ | 2 | −2.444293750583 | 0.000129601311 | - |
| {0,0,2,0,0,0} | $1_3$ | 2 | −1.111855930538 | 0.000011727787 | 0.000012785580 |
| {0,1,0,1,0,0} | $0_2 0_4$ | 2 | −1.560671012472 | 0.000330572718 | - |

**Table C2.** All Bethe states for $L = 12$ having nonzero overlap with the zero-momentum Majumdar-Ghosh (MG) state. The first column shows the string content of the Bethe states. The second and third column show $2I_n^+$, with $I_n^+$ the BGT quantum numbers identifying the different states, and the number $q$ of independent strings. In the second column only the positive BGT numbers are shown. Note that, in contrast to Table C1 no states with infinite rapidities are present. The fourth column is the Bethe state eigenenergy. Finally, the last two columns show the exact overlap with the MG state and the approximate result obatained using the BGT equations. In the last column Bethe states containing zero-momentum strings are excluded. Deviations from the exact result (digits with different colors) are attributed to the string hypothesis.

324 (2007).
[5] S. Trotzky, Y.-A. Chen, A. Flesch, I. P. McCulloch, U. Schollwöck, J. Eisert, and I. Bloch, Nature

Phys. **8**, 325 (2012).
[6] M. Gring, M. Kuhnert, T. Langen, T. Kitagawa, B. Rauer, M. Schreitl, I. Mazets, D. A. Smith, E. Demler, and J. Schmiedmayer, Science **337**, 6100 (2012).
[7] M. Cheneau, P. Barmettler, D. Poletti, M. Endres, P. Schaua, T. Fukuhara, C. Gross, I. Bloch, C. Kollath, and S. Kuhr, Nature (London) **481**, 484 (2012).
[8] U. Schneider, L. Hackeruller, J. P. Ronzheimer, S. Will, S. Braun, T. Best, I. Bloch, E. Demler, S. Mandt, D. Rasch, and A. Rosch, Nature Phys. **8**, 213 (2012).
[9] M. Kuhnert, R. Geiger, T. Langen, M. Gring, B. Rauer, T. Kitagawa, E. Demler, D. Adu Smith, and J. Schmiedmayer, Phys. Rev. Lett. **110**, 090405 (2013).
[10] T. Langen, R. Geiger, M. Kuhnert, B. Rauer, and J. Schmiedmayer, Nature Phys. **9**, 640 (2013).
[11] F. Meinert, M. J. Mark, E. Kirilov, K. Lauber, P. Weinmann, A. J. Daley, and H.-C. Nagerl, Phys. Rev. Lett. **111**, 053003 (2013).
[12] T. Fukuhara, A. Kantian, M. Endres, M. Cheneau, P. Schaua, S. Hild, C. Gross, U. Schollwöck, T. Giamarchi, I. Bloch, and S. Kuhr, Nature Phys. **9**, 235 (2013).
[13] J. P. Ronzheimer, M. Schreiber, S. Braun, S. S. Hodgman, S. Langer, I. P. McCulloch, F. Heidrich-Meisner, I. Bloch, and U. Schneider, Phys. Rev. Lett. **110**, 205301 (2013).
[14] S. Braun, M. Friesdorf, S. Hodgman, M. Schreiber, J. Ronzheimer, A. Riera, M. del Rey, I. Bloch, J. Eisert, and U. Schneider, PNAS **112**, 3641 (2015).
[15] T. Langen, S. Erne, R. Geiger, B. Rauer, T. Schweigler, M. Kuhnert, W. Rohringer, I. E. Mazets, T. Gasenzer, J. Schmiedmayer, Science **348**, 6231 (2015).
[16] A. Polkovnikov, K. Sengupta, A Silva, and M. Vengalattore, Rev. Mod. Phys. **83**, 863 (2011).
[17] P. Calabrese and P. Le Doussal, J. Stat. Mech. (2014) P05004.
[18] V. Alba, arXiv:1507.06994.
[19] H. Bethe, Zur Theorie der Metalle. I. Eigenwerte und Eigenfunktionen der linearen Atomkette, Z. Phys. **71**, 205 (1931).
[20] M. Takahashi, *Thermodynamics of one-dimensional solvable models*, Cambridge University Press, Cambridge, 1999.
[21] V. E. Korepin, N. M. Bogoliubov, and A. G. Izergin, *Quantum Inverse Scattering Methods and Correlation Functions*, Cambridge University Press, Cambridge, 1997.
[22] M. Brockmann, J. De Nardis, B. Wouters, and J.-S. Caux, J. Phys. A: Math. Theor. **47**, 345003 (2014).
[23] M. Brockmann, J. De Nardis, B. Wouters, and J.-S. Caux, J. Phys. A: Math. Theor. **47**, 145003 (2014).
[24] M. Brockmann, J. Stat. Mech. (2014) P05006.
[25] B. Pozsgay, J. Stat. Mech. (2014) P06011.
[26] P. Calabrese and J.-S. Caux, Phys. Rev. Lett. **98**, 150403 (2007).
[27] P. Calabrese and J.-S. Caux, J. Stat. Mech. P08032 (2007).
[28] J. De Nardis, B. Wouters, M. Brockmann, and J.-S. Caux, Phys. Rev. A **89**, 033601 (2014).
[29] B. Pozsgay, M. Mestyán, M. A. Werner, M. Kormos, G. Zaránd, and G. Takács, Phys. Rev. Lett. **113**, 117203 (2014).
[30] B. Wouters, M. Brockmann, J. De Nardis, D. Fioretto, M. Rigol, and J.-S. Caux, Phys. Rev. Lett. **113**, 117202 (2014).
[31] M Mestyán, B. Pozsgay, G. Takács, and M. A. Werner, J. Stat. Mech. (2015) P04001.
[32] E. Ilieveski, J. De Nardis, B. Wouters, J.-S. Caux, F. H. Essler, and T. Prosen, arXiv:1507.02993.
[33] M. Brockmann, B. Wouters, D. Fioretto, J. De Nardis, R. Vlijm, and J.-S. Caux, J. Stat. Mech. (2014) P12009.
[34] P. P. Mazza, J.-M. Stéphan, E. Canovi, V. Alba, M. Brockmann, and M. Haque, arXiv:1509.04666.
[35] M. Fagotti and F. H. Essler, J. Stat. Mech. (2013) P07012.
[36] M. P. Grabowski and P. Mathieu, Ann. Phys. N.Y. **243**, 299 (1995).
[37] M. H. Quenouille, Ann. Math. Statist. **20**, 355 (1949).
[38] U. Wolff, Comput. Phys. Comm. **156**, 143 (2004).

[39] L. Piroli and P. Calabrese, J. Phys. A **47**, 385003 (2014).